Electromagnetic Bicycle Damper (EMBR) Non-Linear Estimation Implementation

Edward Silva

***Abstract*—This project explores the development of a non-linear estimation strategy for the Electromagnetic Mountain Bike Response (EMBR) suspension system. The system uses magnetorheological (MR) fluid within a redesigned front-fork damper system featuring an internal electromagnetic coil and an annular gap to achieve variable damping reactions to given force inputs.**

I. Introduction

The goal of this project is to develop and evaluate an estimation strategy for an electromagnetic mountain bike suspension damper (EMBR). Traditional mountain bike suspension relies on mechanical valving and shim stacks whose fixed geometry cannot adapt to varying terrain without manual adjustment. The EMBR system addresses this limitation by utilizing magnetorheological (MR) fluid whose yield stress changes under an applied magnetic field, enabling variable damping forces matched to riding conditions. Because key internal quantities that define performance are not directly measurable with low-cost sensors, an estimator is needed to infer these states from available sensor measurements.

II. System Description

The system is illustrated in Figure 1. The front suspension is modeled as a mass spring damper system with the custom MR damper placed between the "sprung" bicycle frame and the "unsprung" lower fork assembly. The physical damper system includes an electromagnet core and coil, an internal floating piston (IFP), and a main rebound piston that forces MR fluid through a narrow annular gap. A control system consisting of a microcontroller, MOSFET-based power regulation, battery, dual accelerometers, and a linear string potentiometer measures the system dynamics.

The vertical motion of the suspension is described by the displacement $z(t)$, also known as the position of the piston between the sprung and unsprung masses, in meters, and its time derivative the piston velocity, $\dot{z}(t)$, in m/s. An effective magnetic field intensity $h(t)$, in A/m, represents the internal electromagnetic state of the MR fluid. The electromagnetic coil is driven by a control input $u(t)$. Terrain and rider loading on the wheel are lumped into an unmeasured disturbance force $F_{\text{in}}(t)$ acting on the equivalent mass. To accurately reflect real-world riding conditions in simulation, $F_{\text{in}}(t)$ is characterized as a superposition of harmonic base trail roughness, stochastic surface noise, and sharp Gaussian-pulse impacts representing discrete obstacles like large rocks or jump impacts. The damping force generated by the MR fluid and viscous effects opposes the motion and is denoted $F_{\text{damp}}(\dot{z}(t), h(t))$.

III. System State Space Model

The motion of the equivalent sprung mass is determined by a force balance, where

$$m\ddot{z}(t) = F_{\text{in}}(t) - kz(t) - F_{\text{damp}}(\dot{z}(t), h(t)) \tag{1}$$

is defined by the input force $F_{\text{in}}(t)$ driving the suspension downward, resisted by the mechanical spring force $kz(t)$ and the variable damping force $F_{\text{damp}}(\dot{z}(t), h(t))$. The magnetic field intensity $h(t)$ is driven toward a steady-state value determined by the applied current $i(t)$ through a first-order response model that captures the electromagnetic dynamics. This relationship is explicitly governed by the differential equation

$$\dot{h}(t) = -\frac{1}{\tau}h(t) + \frac{1}{\tau}i(t) \tag{2}$$

where τ is the magnetic-field response time constant to changes in the applied current.

The total damping force combines viscous resistance and electromagnetically induced yield stress. The nonlinear damping force is modeled as

$$F_{\text{damp}}(\dot{z}(t), h(t)) = K_{\text{v}}\dot{z}(t) + K_{\text{m}}h(t)\tanh(\alpha\dot{z}(t)), \tag{3}$$

where α is a scaling factor that controls the sharpness of the transition across zero velocity, K_{v} is the viscous damping coefficient, and K_{m} is the magnetic yield constant. The viscous coefficient is derived from the MR fluid's base viscosity and annular gap geometry. The lumped constant K_{m} combines the geometric yield factor K_{geom} with the linearized yield-stress gain K_{τ} of the fluid operating below magnetic saturation.

Substituting Equation (3) into Equation (1) gives,

$$m\ddot{z}(t) = F_{\text{in}}(t) - kz(t) - K_{\text{v}}\dot{z}(t) - K_{\text{m}}h(t)\tanh(\alpha\dot{z}(t)). \tag{4}$$

By linearizing the equation of motion, Equation (4), around an operating point, the following components are used in the state-space Jacobians. A_{22} is the linearized damping term, and A_{23} is the magnetic-yield gain, defined as:

$$A_{22} = \frac{\partial\ddot{z}(t)}{\partial\dot{z}(t)} = -\frac{1}{m}\big(K_{\text{v}} + h(t)K_{\text{m}}\alpha\,\text{sech}^2(\alpha\dot{z}(t))\big),$$

$$A_{23} = \frac{\partial\ddot{z}(t)}{\partial h(t)} = -\frac{K_{\text{m}}}{m}\tanh(\alpha\dot{z}(t))$$

The state vector can be defined as

$$x(t) = \begin{bmatrix} z(t) \\ \dot{z}(t) \\ h(t) \end{bmatrix}. \tag{5}$$

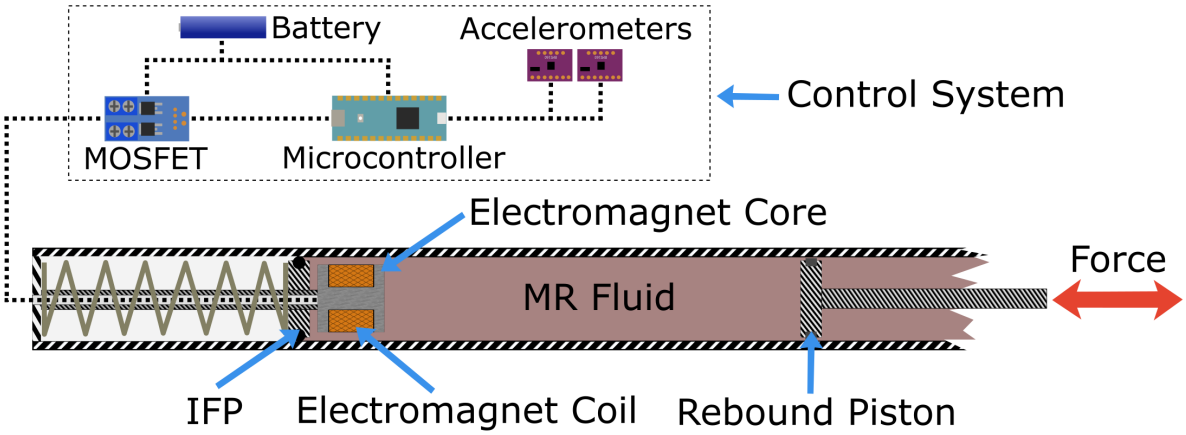

Fig. 1: The functional drawing of the EMBR Damper system [1]

Let the combined input vector, incorporating both the unmeasured disturbance and the control input, be defined as

$$u(t) = \begin{bmatrix} F_{\text{in}}(t) \\ i(t) \end{bmatrix}, \tag{6}$$

where $i(t)$ is the current applied to the electromagnetic coil system

From the definitions above, the complete nonlinear state-space representation can be written as

$$\dot{x}(t) = \begin{bmatrix} 0 & 1 & 0 \\ -\frac{k}{m} & A_{22} & A_{23}(t) \\ 0 & 0 & -\frac{1}{\tau} \end{bmatrix} x(t) + \begin{bmatrix} 0 & 0 \\ \frac{1}{m} & 0 \\ 0 & \frac{1}{\tau} \end{bmatrix} u(t), \tag{7}$$

$$y(t) = \begin{bmatrix} 1 & 0 & 0 \\ -\frac{k}{m} & A_{22} & A_{23}(t) \end{bmatrix} x(t) + \begin{bmatrix} 0 & 0 \\ \frac{1}{m} & 0 \end{bmatrix} u(t). \tag{8}$$

IV. Estimation Scenario

The goal of this project is to estimate $z(t)$, $\dot{z}(t)$, and $h(t)$ in order to characterize the damping behavior of the EMBR system during operation. In this scenario the state measurements, as described in Section III, are corrupted by noise, modeled as a zero-mean independent and identically distributed (iid) Gaussian random sequence.

Unmeasured disturbances include the terrain and rider forces lumped into $F_{\text{in}}(t)$, as well as unmodeled effects such as pivot friction and frame compliance, which will be treated as process noise in the state-space model.

The estimation experiment will begin with the bicycle already in motion, so the initial states are uncertain. The specific assumed distributions and values for the initial position $z(0)$, initial velocity $\dot{z}(0)$, and initial magnetic field intensity $h(0)$ are detailed alongside the system parameters in Table I.

V. Simulation of Estimation Scenario

A simulation of the estimation scenario was performed using MATLAB and Simulink. The continuous-time system dynamics defined by Equation (7) were solved numerically, with the random number generators and solver operating at a sample time of $T_s = 0.01$ s. The system parameters were chosen as shown in Table I.

Parameter	Value	Units
T_s	0.01	s
m	100	kg
k	10000	N/m
K_{v}	1000	N·s/m
K_{m}	0.005	
α	100	s/m
N_{turns}	160	
g_{gap}	0.001	m
$\sigma_{\dot{z}}^2$	0.005	$(\text{m/s})^2$
σ_z^2	5.0×10^6	m^2
σ_a^2	0.1	$(\text{m/s}^2)^2$
Q_s	5000000	N^2
τ	0.05	s
$z(0)$	$\mathcal{N}(0, 0.01)$	m
$\dot{z}(0)$	$\mathcal{N}(0, 0.01)$	m/s
$h(0)$	1.0	A/m

Table I: System parameters chosen for the simulation

To test the estimator, the unmeasured disturbance force $F_{\text{in}}(t)$ was modeled to reflect a realistic terrain profile, shown in Figure 2. As described in Section II, the profile of $F_{\text{in}}(t)$ is comprised of:

1) Harmonic trail roughness consisting of a primary frequency of 1.5 Hz and high-frequency chatter at 8.0 Hz
2) Stochastic surface noise generated using a zero-mean Gaussian random sequence
3) Discrete obstacles modeled as Gaussian pulses, specifically simulating large impacts at $t = 1.0$ s and $t = 2.0$ s

Then, dynamic control input $i(t)$ was programmed to apply a soft base current of 1 A during standard trail chatter, stepping to a stiffer 2 A when the defined obstacle forces exceed 750 N.

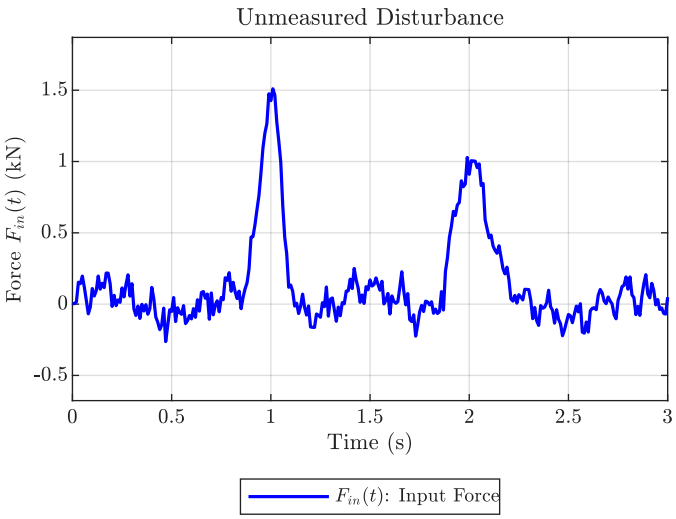

Fig. 2: Unmeasured Disturbance $F_{\text{in}}(t)$

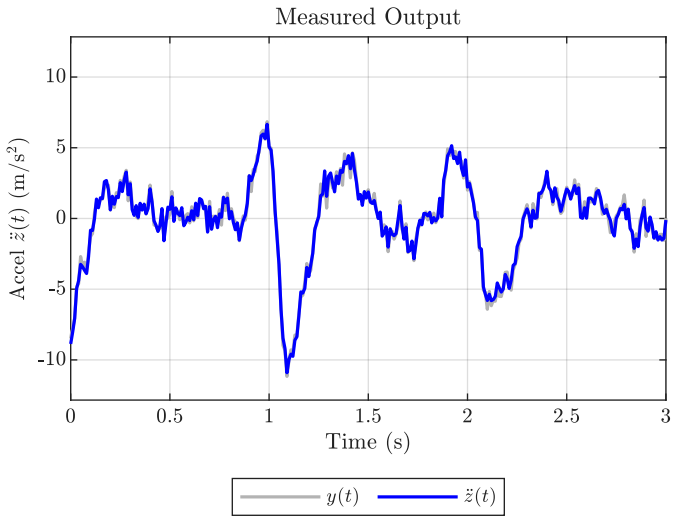

Fig. 3: Measured Output $y(t)$

The state trajectories, $z(t)$, $\dot{z}(t)$, and $h(t)$, were calculated from the resulting simulation and are shown in Figure 4. The internal state trajectories and measured acceleration channel of $y(t)$ are shown in Figure 3.

As seen in Figure 4, the step increases in the control current $i(t)$ during the obstacle impacts at $t = 1.0$ s and $t = 2.0$ s drive a rapid, first-order response in the magnetic field $h(t)$. This temporary spike in magnetic yield stress effectively stiffens the damper, which suppresses the peak piston velocity $\dot{z}(t)$ and suspension displacement $z(t)$ during the major terrain hits. The measured acceleration channel of $y(t)$ shown in Figure 3 captures these high-force events despite the presence of the simulated zero-mean sensor noise.

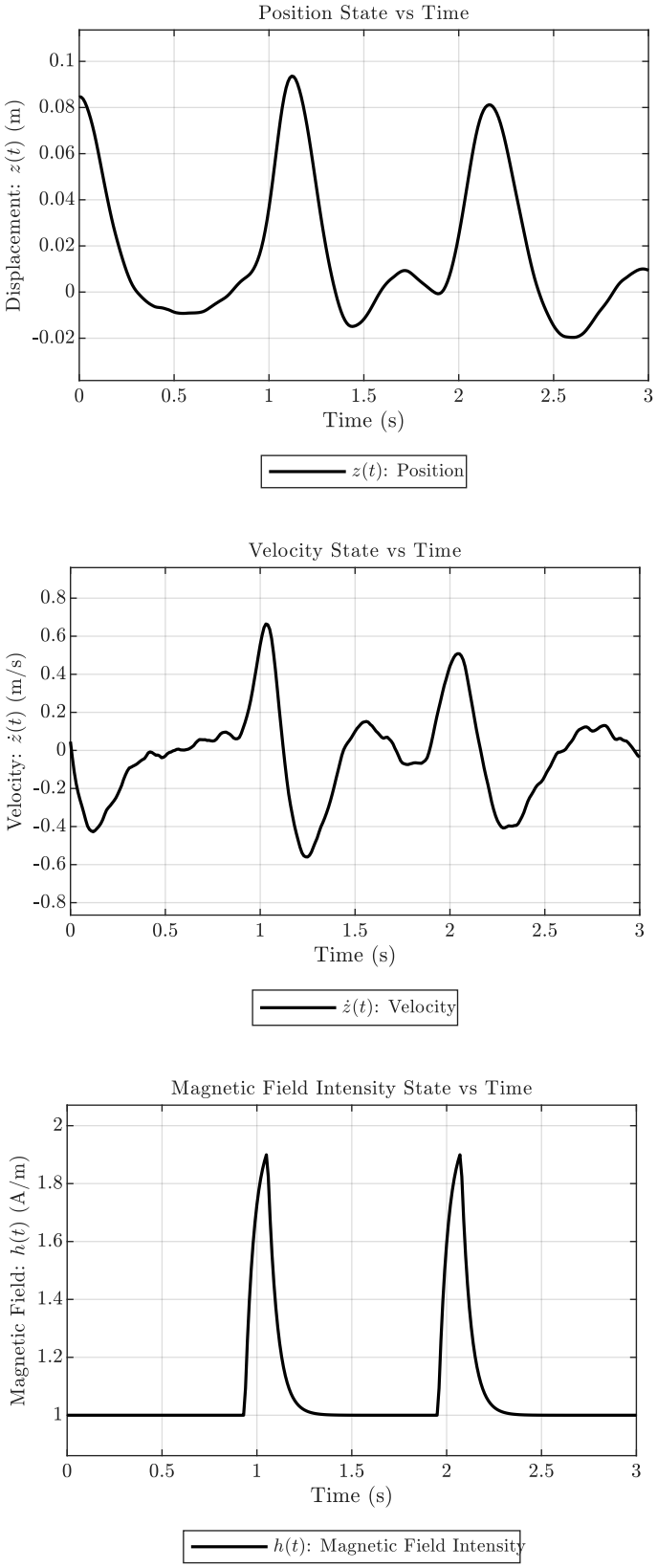

Fig. 4: Internal state trajectories from the terrain profile.

VI. Disturbance Modelling

The unmeasured terrain force $F_{\text{in}}(t)$ is modeled as a discrete random walk to capture dynamic obstacle impacts. Assuming a uniform sample time T_s, the disturbance state is updated as

$$F_{\text{in},k+1} = F_{\text{in},k} + s_k \tag{9}$$

where s_k is a zero-mean independent and identically distributed (iid) Gaussian random sequence with variance Q_s. Combining the physical system states with this discrete disturbance yields the augmented state vector $\tilde{x}_k \in \mathbb{R}^4$:

$$\tilde{x}_k = [z_k,\ \dot{z}_k,\ h_k,\ F_{\text{in},k}]^T \tag{10}$$

Applying an Euler approximation, the discrete-time nonlinear state-space representation is

$$\tilde{x}_{k+1} = f(\tilde{x}_k, i_k) + w_k \tag{11}$$

$$y_k = g(\tilde{x}_k) + n_k \tag{12}$$

where i_k is the control current, $w_k = [0, w_{\dot{z},k}, 0, s_k]^T$ is the process noise vector with covariance

$$Q = \begin{bmatrix} 0 & 0 & 0 & 0 \\ 0 & \sigma_{\dot{z}}^2 & 0 & 0 \\ 0 & 0 & 0 & 0 \\ 0 & 0 & 0 & Q_s \end{bmatrix}, \tag{13}$$

and $n_k = [n_{z,k}, n_{a,k}]^T$ is the measurement noise vector with covariance

$$R = \begin{bmatrix} \sigma_z^2 & 0 \\ 0 & \sigma_a^2 \end{bmatrix}. \tag{14}$$

The non-zero $w_{\dot{z},k}$ term accounts for unmodeled physical dynamics.

At the 8.0 Hz chatter component and $T_s = 0.01$ s sampling, this introduces a small phase lag (approximately 2.8° per sample) and is treated as a modeling limitation.

The discrete state transition function $f(\tilde{x}_k, i_k)$ gives the true nonlinear system dynamics as

$$f(\tilde{x}_k, i_k) = \tilde{x}_k + T_s \begin{bmatrix} \tilde{x}_{2,k} \\ a_k(\tilde{x}_k) \\ -\frac{1}{\tau}\tilde{x}_{3,k} + \frac{1}{\tau} i_k \\ 0 \end{bmatrix} \tag{15}$$

where the nonlinear acceleration $a_k(\tilde{x}_k)$ is defined as

$$a_k(\tilde{x}_k) = -\frac{k}{m}\tilde{x}_{1,k} - \frac{K_{\text{v}}}{m}\tilde{x}_{2,k} - \frac{K_{\text{m}}}{m}\tilde{x}_{3,k}\tanh(\alpha\tilde{x}_{2,k}) + \frac{1}{m}\tilde{x}_{4,k}.$$

Because the input force is now within the augmented state, the discrete measurement function $g(\tilde{x}_k)$ describing the displacement and acceleration output is defined as

$$g(\tilde{x}_k) = \begin{bmatrix} \tilde{x}_{1,k} \\ a_k(\tilde{x}_k) \end{bmatrix}. \tag{16}$$

To propagate the state covariance matrix during the Extended Kalman Filter (EKF) prediction step, the Jacobian matrix $F_k = \frac{\partial f}{\partial \tilde{x}}\big|_{\tilde{x}_k}$ is evaluated utilizing the continuous-time partial derivatives A_{22} and A_{23} previously established in Section III. The measurement Jacobian matrix H_k maps the augmented state to the dual-sensor output, shown as

$$H_k = \begin{bmatrix} 1 & 0 & 0 & 0 \\ -\frac{k}{m} & A_{22} & A_{23} & \frac{1}{m} \end{bmatrix} \tag{17}$$

Assuming the estimation begins with the bicycle in motion on flat terrain, the initial disturbance force is nominally zero. The initial augmented state $\tilde{x}_0$ is defined as a Gaussian random variable with mean and covariance, given by

$$E[\tilde{x}_0] = \begin{bmatrix} 0 \\ 0 \\ 1.0 \\ 0 \end{bmatrix}, \quad C_{\tilde{x}_0} = \begin{bmatrix} 0.01 & 0 & 0 & 0 \\ 0 & 0.01 & 0 & 0 \\ 0 & 0 & 0.01 & 0 \\ 0 & 0 & 0 & 100 \end{bmatrix} \tag{18}$$

VII. Estimation Using Extended Kalman Filter

The Extended Kalman Filter (EKF) is applied to estimate the conditional distributions of the states of the system described by Equation (11), Equation (12), and Equation (16). The filter is initialized at time $k = 0$ with $\hat{x}_0 = E[\tilde{x}_0]$ and $P_0 = C_{\tilde{x}_0}$, as detailed in Section VI.

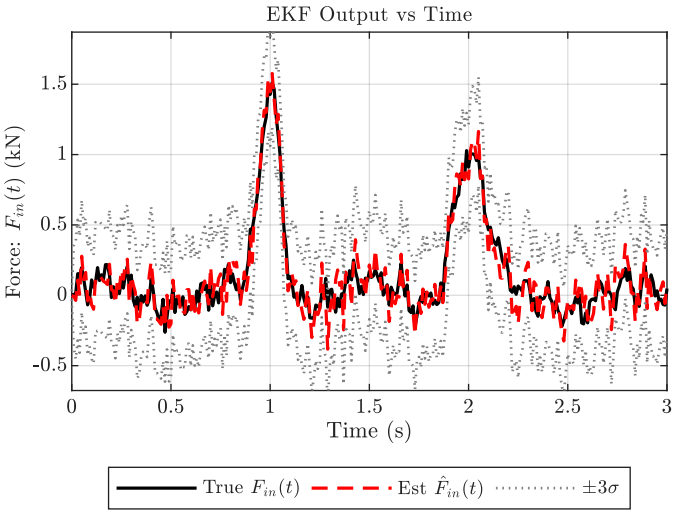

Fig. 5: Measured EKF Output $y(t)$

The state estimation was performed using the measured output vector $y(t)$, which combines the string potentiometer displacement and accelerometer data. Figure 6 display the true system states plotted against the EKF state estimates, along with the calculated $\pm 3\sigma$ uncertainty bounds derived from the diagonal elements of the state error covariance matrix P_k.

As seen in the results, Figure 5, the EKF successfully tracks the low-frequency and primary harmonic terrain variations for displacement and velocity. The estimated magnetic field tightly matches the true unmeasured magnetic state, validating the first-order electromagnetic response model.

However, during the highly nonlinear high-force impacts at $t = 1.0$ s and $t = 2.0$ s, the uncertainty bounds temporarily widen. The disturbance force estimator exhibits a slight phase lag compared to the true stochastic terrain profile, primarily

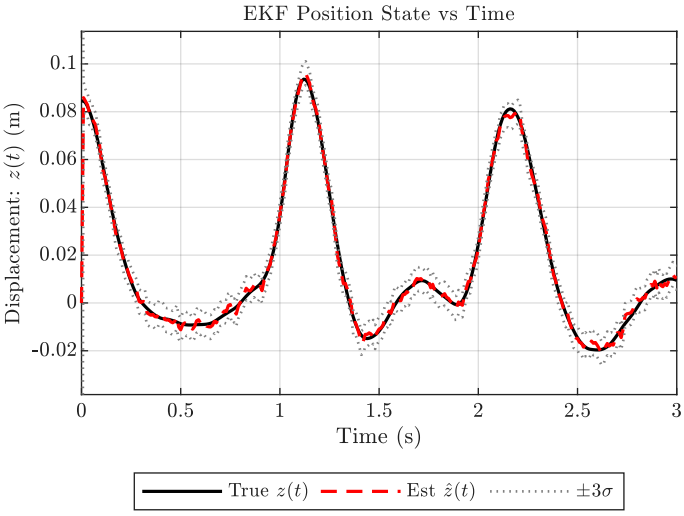

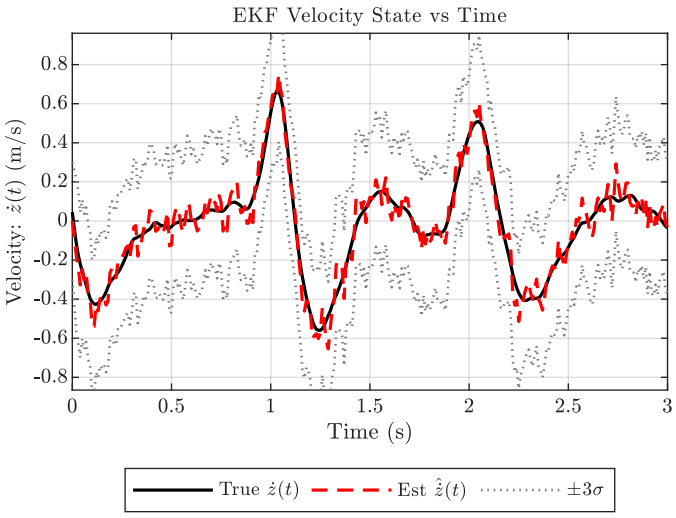

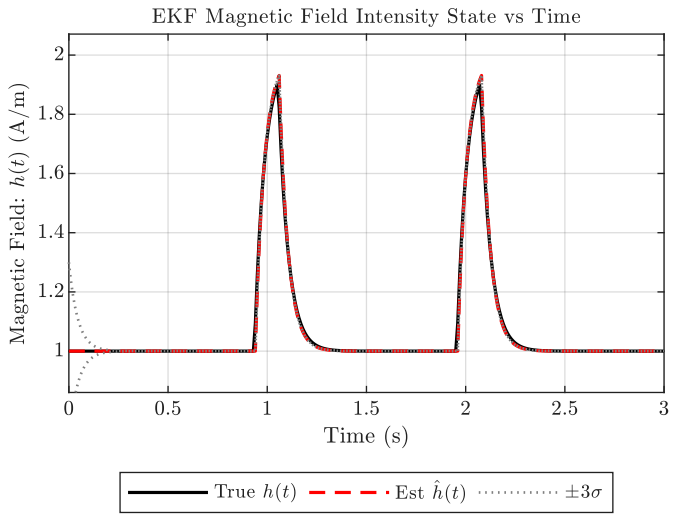

Fig. 6: Internal EKF state trajectories from the terrain profile.

due to the discrete approximation of the unmodeled high-frequency chatter components at 8.0 Hz. The state error covariance analysis confirms that the errors remain bounded within the 3σ confidence intervals over the entire experiment, indicating an observable nonlinear tracking performance.

VIII. Estimation Using Unscented Kalman Filter

Because the damper dynamics involve highly nonlinear terms, specifically in the hyperbolic tangent function characterizing the MR fluid yield transition, an Unscented Kalman Filter (UKF) was also implemented to evaluate potential improvements over the EKF. The UKF uses the unscented transform to propagate selected sigma points through the true nonlinear functions $f(\tilde{x}_k, i_k)$ and $g(\tilde{x}_k)$, capturing the posterior mean and covariance accurately for Gaussian inputs.

The UKF implementation utilizes a deterministic sampling technique known as the unscented transform to represent the state distribution using a minimal set of $2L+1$ carefully chosen sigma points, where $L = 4$ is the augmented state dimension. These points are propagated through the true nonlinear system dynamics, avoiding the truncation errors associated with analytical linearization. The specific scaling parameters and weights governing the spread and recombination of these sigma points were selected to optimize for the assumed Gaussian distributions, and are detailed in Table II.

Parameter	Value	Description
L	4	Augmented state dimension
α_{ukf}	1×10^{-3}	Primary spread scaling factor
κ	0	Secondary scaling factor
β	2	Gaussian distribution optimal weight
λ	$\alpha_{\text{ukf}}^2(L+\kappa) - L$	Composite scaling factor
$W_m^{(0)}$	$\frac{\lambda}{L+\lambda}$	Mean weight (center point)
$W_c^{(0)}$	$W_m^{(0)} + (1 - \alpha_{\text{ukf}}^2 + \beta)$	Covariance weight (center point)
$W_m^{(i)}, W_c^{(i)}$	$\frac{1}{2(L+\lambda)}$	Surrounding point weights ($i = 1 \dots 2L$)

Table II: UKF Unscented Transform Parameters

The UKF results, shown in Figure 8, utilize the same process and measurement noise covariance matrices (Q and R) as the EKF to ensure a valid comparison. The UKF shows improved robustness during velocity zero-crossings, where the $\tanh(\alpha\dot{z}(t))$ gradient in the EKF Jacobian undergoes rapid changes that can momentarily increase the covariance.

By avoiding analytical linearization, the UKF provides tighter $\pm 3\sigma$ error bounds on the disturbance force $F_{\text{in}}(t)$ and velocity $\dot{z}(t)$ estimates during high-frequency stochastic chatter. The EKF relies on a first-order Jacobian approximation, which introduces errors when evaluating the highly nonlinear $\tanh(\alpha\dot{z}(t))$ MR fluid yield transition. The UKF's unscented transform directly moves sigma points through the true nonlinear equations, effectively capturing higher-order moments of the state distribution. This reduction in linearization error produces a tightly bounded state error covariance

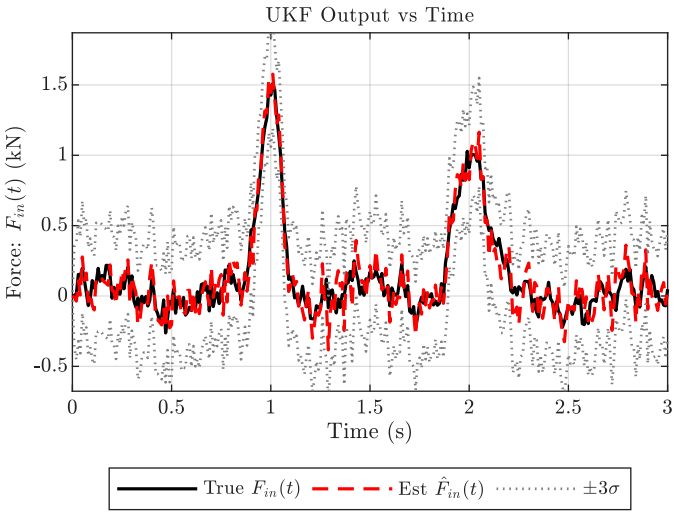

Fig. 7: Measured UKF Output $y(t)$

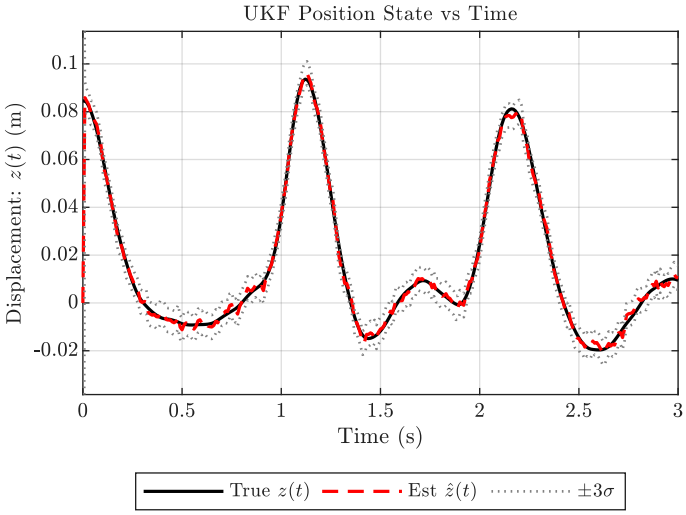

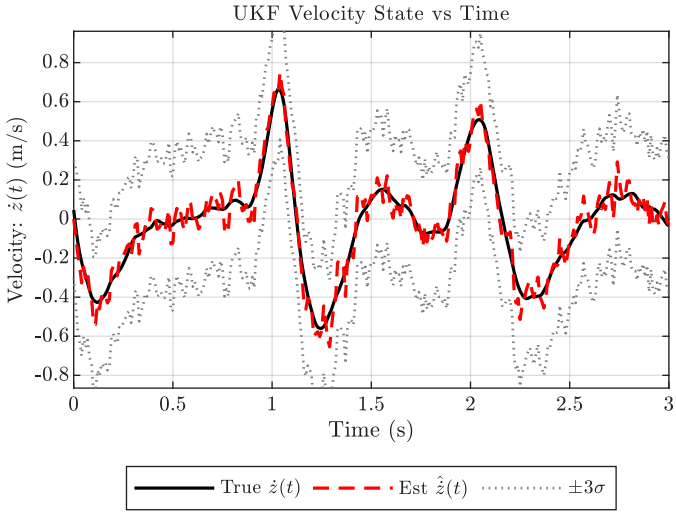

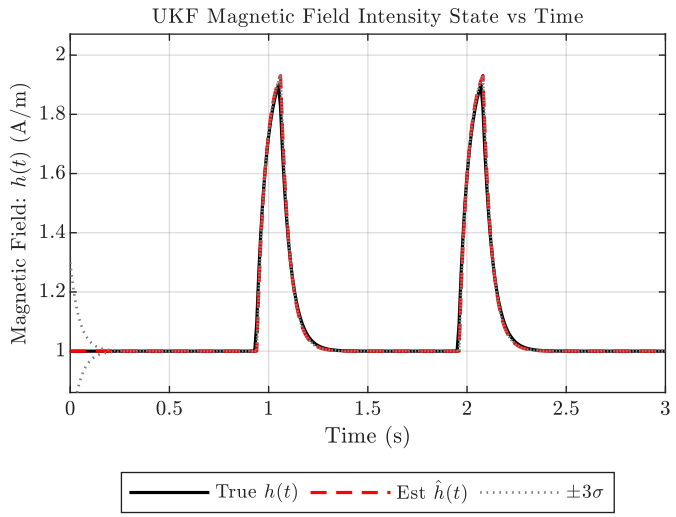

Fig. 8: Internal UKF state trajectories from the terrain profile.

matrix P_k, making the UKF a better candidate for a real-world implementation.

IX. Conclusion

A nonlinear estimation strategy utilizing an Extended and Unscented Kalman Filter was successfully developed for the EMBR suspension system. The system's unique combination of mechanical springs, viscous damping, and magnetorheological fluid yield stress provide a variable damping response that reacts to changing terrain profiles. A complete continuous and discrete state-space formulation was developed, incorporating unmeasured environmental disturbances directly into an augmented state vector.

An Extended Kalman Filter was implemented to infer internal operational states, these being, displacement, velocity, magnetic field intensity, and input disturbance forces from a noisy string potentiometer and dual-accelerometer measurement system. Simulation results verified the estimator's effectiveness, as the tracking performance maintained strict adherence to the theoretical $\pm 3\sigma$ covariance bounds, confirming observability.

Future work will focus on deploying this UKF estimation strategy in a real-time embedded microcontroller context to evaluate its computational feasibility and overhead against the EKF.

References

[1] B. Mackenzie et al., "Capstone design project: EMBR – team 73," Colorado School of Mines, Golden, CO, Feb. 2026, Project sponsored by ARUS MR TECH.